

# The Capacitance-Power-Hysteresis Trilemma in Nanoporous Supercapacitors

Alpha A Lee,<sup>1,2</sup> Dominic Vella,<sup>2</sup> Alain Goriely,<sup>2</sup> and Svyatoslav Kondrat<sup>3,4</sup>

<sup>1</sup>*John A. Paulson School of Engineering and Applied Sciences,  
Harvard University, Cambridge, MA 02138, USA*

<sup>2</sup>*Mathematical Institute, Andrew Wiles Building, University of Oxford,  
Woodstock Road, Oxford OX2 6GG, United Kingdom*

<sup>3</sup>*IBG-1: Biotechnology, Forschungszentrum Jülich, 52425 Jülich, Germany*

<sup>4</sup>*Department of Chemistry, Faculty of Natural Sciences, Imperial College London, SW7 2AZ, UK*

Nanoporous supercapacitors are an important player in the field of energy storage that fill the gap between dielectric capacitors and batteries. The key challenge in the development of supercapacitors is the perceived tradeoff between capacitance and power delivery. Current efforts to boost the capacitance of nanoporous supercapacitors focus on reducing the pore size so that they can only accommodate a single layer of ions. However, this tight packing compromises the charging dynamics and hence power density. We show via an analytical theory and Monte Carlo simulations that charging is sensitively dependent on the affinity of ions to the pores, and that the capacitance of ionophobic pores can be optimized at pore widths significantly larger than the ion diameter. Our theory also predicts that charging can be hysteretic with a significant energy loss per cycle for intermediate ionophilicities. We use these observations to explore the parameter regimes in which a capacitance-power-hysteresis *trilemma* may be avoided.

## I. INTRODUCTION

The physics of charge storage at the nanoscale has received significant attention in recent years due to its relevance for efficient energy storage and the development of novel green technologies [1–3]. In particular, extensive effort has been channeled into studying electrical double layer capacitors (also called supercapacitors) in which energy is stored at the electrode-electrolyte interface. Their importance for energy storage has stimulated the development of novel techniques for fabrication of conducting nanoporous materials [3, 4]. For instance, high-temperature chlorination of carbides produces carbon electrodes with a network of slit and/or cylindrical nanopores with narrow pore-size distribution about a well-controlled average pore size [5]. There is also an emerging class of graphene- and MXene-based electrodes consisting of aligned slit nanopores with pore sizes comparable to the ion diameter [6–8]. Additionally it is possible to manipulate the ion-pore interactions by functionalising carbons. For instance, preparing carbon nanofibers in the presence of potassium hydroxide changes the surface functionality and increases the ion-pore attraction [9].

Nanoporous supercapacitors benefit from high surface-to-volume ratio of these materials with an increase in the volumetric capacitance observed as the surface area of the electrode increases [10]. However, pioneering experiments [11–14] have shown that a drastic increase in *surface-specific* capacitance is achieved when the average pore size approaches the ion diameter. Using a model of single metallic slit-shaped nanopore (*c.f.* Figure 1), this ‘anomalous’ increase of capacitance has been explained by the emergence of a ‘superionic state’ in which the inter-ionic interactions become exponentially screened [15]. Decreasing the pore size promotes screening [16–18] which decreases the energy penalty for pack-

ing like charges and unbinding ion pairs, purportedly leading to an increase in the capacitance.

This effect of metallic screening has been observed in molecular dynamics simulations that use more elaborate models to account for complex pore geometries [19, 20] and realistic ions [21–23]. If metallic screening is the sole driver of increased capacitance, the capacitance can only be optimized when the pore size equals the ion size. However, such a close-fitting pore is detrimental to the charging dynamics [24] because of the reduced effective diffusivity [25, 26] and because the kinetic barrier to pore entry is large. Increased capacitance therefore appears to come at the cost of prolonged charging. This leads to a dilemma in the design of supercapacitors — should the design be chosen to optimize capacitance or power? Alternatively, one might naturally ask: Can the capacitance be maximized away from such close-fitting pores?

It is known that charging of flat electrodes may show a *hysteresis* [27–29], *i.e.* the differential capacitance depends on the initial voltage and the direction of scan [27, 30]. This is connected with the existence of two or more metastable states of an ionic liquid at the electrode surface. In nanoconfinement, there is evidence from a mean-field study [15], Monte Carlo [31] and molecular dynamics [32, 33] simulations that charging of slit nanopores can proceed via a voltage-induced discontinuous transition that is manifested by an abrupt change in the ion density. Such discontinuous transitions can be detrimental to because of *hysteretic energy losses* when the charging and discharging routes follow different metastable branches. It is thus important to know whether (and when) charging is hysteretic, and how hysteresis might be avoided altogether. This adds another dimension to the dilemma already mentioned.

To answer these questions, we combine a mean field theory with Monte Carlo simulations for a model slit nanopore (Figure 1). We consider monovalent ions and a

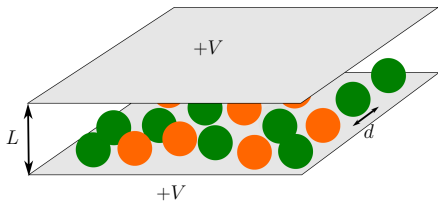


FIG. 1: Schematic drawing of the model porous electrode under consideration: Ions of diameter  $d$  are confined between two metallic surfaces separated by a distance  $L$ . A potential  $V$  (relative to the bath) is applied.

single slit-shaped metallic nanopore. The pore entrance and closing are ignored, and charging is modelled by applying a non-zero potential to the pore walls. This or similar models have previously been used to study charge storage [15, 23, 31, 34–38] and the dynamics of charging [25, 26] of nanoporous supercapacitors. Here, we focus specifically on pores whose sizes are comparable with the ion diameter. In this limit, the system is quasi two-dimensional, and we can assume that ions are located on the central symmetry plane of the pore. This allows us to develop a mean-field theory in two dimensions, whereby, improving on a model developed previously [15], the out-of-plane packing of ions (for  $L > d$ ) is taken into account by introducing an effective pore-width dependent ion diameter  $d^* \leq d$  (see Appendix A). We supplement and compare our mean-field results with grand canonical Monte Carlo simulations of the same system in three dimensions (for simulation details see Appendix B).

The model employed here ignores the chemical details of ions and the complex structures of nanoporous electrodes. With these deliberate simplifications we aspire to reveal and understand the essential physics at work, without the complexity of real supercapacitors. In particular, our study reveals that contrary to the long-standing paradigm, a maximal capacitance can actually be achieved when pores are appreciably *wider* than the ion diameter. In addition, we show that there is, in general, charging hysteresis with significant energy loss per cycle. However, this hysteresis can be evaded by carefully tuning the ion-pore interaction energy. This study therefore reveals generic features of such systems that we believe should apply more generally and hence may provide a framework within which to design optimal nanoporous supercapacitors and avoid the capacitance-power-hysteresis trilemma.

## II. IONOPHOBICITY OF PORES

Our primary interest is to determine how the affinity of ions towards pores affects charging. In our model, affinity is controlled by the electrochemical potential,

$$h_{\pm} = \pm eV + \delta E_{\text{self}} + \delta E_{\pm}, \quad (1)$$

where  $V$  is the applied voltage,  $e$  the elementary charge,  $\delta E_{\text{self}}$  the ions' self-energy (see Appendix A), and  $\delta E_{\pm}$  the resolution energy [15]. The resolution energy is the energy of transferring an ion from the bulk to the pore, and includes here the chemical potential of ions in the bulk. We assume  $\delta E_{+} = \delta E_{-} = \delta E$  for simplicity.

At zero applied voltage,  $h_{\pm} = h_0 = \delta E_{\text{self}} + \delta E$  and the sign of  $h_0$  determines whether the ion-pore interactions are favourable. For pores with  $h_0 > 0$  (unfavourable ion-pore interaction), the occupancy of the pore at zero applied voltage is expected to be low: we therefore refer to such pores as *ionophobic*. For large positive  $h_0$  the pore will be (almost) completely free of ions at zero applied voltage: we therefore refer to such pores as *strongly ionophobic*. Conversely pores with  $h_0 < 0$  will be termed *ionophilic*, and a large negative  $h_0$  will correspond to *strongly ionophilic* pores, which are nearly fully occupied by ions at no applied voltage.  $h_0 = 0$  marks the crossover between *ionophilic* and *ionophobic* behaviours, which therefore occurs at a resolution energy  $\delta E = \delta E_{\text{crossover}} = -\delta E_{\text{self}}$ . For instance, for a 1nm wide pore and a typical Bjerrum length of 25nm, we have  $\delta E_{\text{crossover}} \approx 17 k_B T$  (see Appendix A for an estimate of  $\delta E_{\text{self}}$ ).

To obtain an estimate for the resolution energy, we decompose  $\delta E$  into  $\delta E \approx \delta E_{\text{desolv}} + \delta E_{\text{non-ele}}$ , where  $\delta E_{\text{desolv}}$  is the desolvation energy of the bulk ionic liquid (transferring one solvated ion from the bulk liquid to the vapour state), and  $\delta E_{\text{non-ele}}$  is the ion-pore non-electrostatic interactions (ion-pore electrostatic interactions are accounted for in  $\delta E_{\text{self}}$ ). A combination of quantum mechanical density functional and molecular dynamics simulations [39] suggests  $\delta E_{\text{desolv}} \approx 75 - 100 k_B T$  per ion [63]. The main source of non-electrostatic interactions is the van der Waals attraction, of magnitude  $\delta E_{\text{vdW}} \approx -65 k_B T$  [64]. We thus find that, roughly,  $10 \lesssim \delta E / (k_B T) \lesssim 35$  (note that the crossover between ionophobic and ionophilic pores,  $\delta E_{\text{crossover}}$ , lies in this range). We stress that this range is not exhaustive as other physical effects (*e.g.* specific surface chemistry of the pore) are not taken into account; the definitive metric of ionophilicity/-phobicity is the occupancy of the pore at zero applied voltage.

## III. SEARCHING FOR MAXIMAL CAPACITANCE

The key quantity characterizing the low voltage capacitance response of a supercapacitor is the differential capacitance at zero voltage,

$$C_{D0} = \left. \frac{dQ}{dV} \right|_{V=0}, \quad (2)$$

where  $Q$  is the charged stored in a pore, and  $V$  is the applied potential. In the following discussion, we compute  $Q(V)$  via free energy minimisation, either through

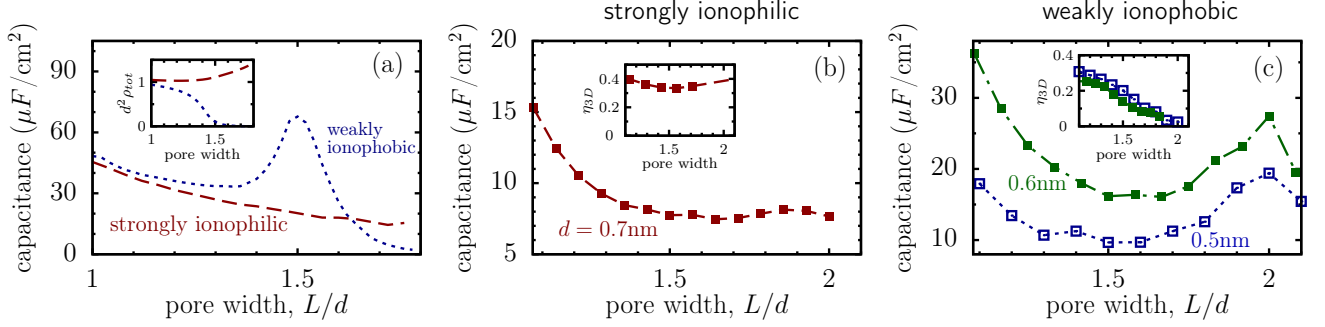


FIG. 2: The differential capacitance at zero voltage as a function of pore width. (a) Results from the mean field theory, plotted for weakly ionophobic ( $\delta E = 25k_B T$ ) and strongly ionophilic ( $\delta E = 10k_B T$ ) pores. The ion diameter is 0.5nm. The inset shows how the total ion density at zero voltage depends on pore width. (b)-(c) Results from Monte Carlo simulations for a strongly ionophilic pore ( $\delta E = -2.5k_B T$ ) and for weakly ionophobic pores ( $\delta E = 38.5k_B T$  for  $d = 0.5\text{nm}$  and  $\delta E = 33.2k_B T$  for  $d = 0.6\text{nm}$ ). The insets show the 3D packing fraction  $\eta_{3D} = (\pi/6)\rho d^3$  as a function of pore width.

a mean-field theory or Monte Carlo simulations (as discussed in Appendix B).

The mean-field approximation for the Helmholtz free energy is given by

$$\beta F = U_{\text{el}}(\rho_+, \rho_-) - S(\rho_+, \rho_-) + \sum_{\alpha=\pm} h_{\alpha} \rho_{\alpha}, \quad (3)$$

where  $\beta = (k_B T)^{-1}$  (with  $k_B$  being the Boltzmann constant and  $T$  temperature) and  $\rho_{\pm}$  is the two-dimensional density of  $\pm$  ions.  $k_B T U_{\text{el}}$  is the contribution to the free energy due to electrostatic interactions,  $k_B T S$  is the excluded volume entropic contribution, and we assume that the density of ions in the slit pore is homogeneous (see Appendix A for expressions of  $U_{\text{el}}$  and  $S$ ). To obtain  $Q(V)$  and hence  $C_{D0}$ , we minimize  $F$  over  $\rho_{\pm}$  subject to fixed  $V$ , noting that  $e(\rho_+ - \rho_-)$  is the charge per unit area (with  $e$  the elementary charge).

For strongly ionophilic pores, the capacitance is maximal for the smallest pores possible, in agreement with the conventional view that the capacitance increases monotonically as the pore size decreases [11–14] (dashed line in Figure 2(a)). Surprisingly, however, we find that for weakly ionophobic pores the differential capacitance has a global maximum when the pore width is significantly larger than the ion diameter (though still smaller than  $2d$ ). This behaviour is due to two competing effects: On the one hand, the loss of ion-image interactions and an increase in electrostatic interactions hinders ions from entering the pore. On the other hand, the same factors also render the pore less populated at zero voltage (the inset in Figure 2a). Thus the peak is achieved when the decrease in the total density frees up enough space in the pore that counter-ion insertion becomes entropically favourable. In fact, for narrow and weakly ionophilic pores the charging at low voltages is dominated by swapping coions for counterions and expelling coions; for wider pores, it is the counterion insertion that drives charging.

This charging behaviour is in contrast to strongly ionophilic pores, where total ion density increases with

increasing pore width because the out-of-plane degrees of freedom allow ions to pack more efficiently. Therefore, both entropy and ion-ion as well as ion-image interactions work against charging as the pore size ( $L$ ) increases, and so the capacitance decreases monotonically for increasing  $L$ . The case of strongly ionophobic pores is not considered here — charging commences only when ions can overcome the ionophobicity barrier ( $eV \approx \delta E$ ) and hence the capacitance at zero voltage is low or vanishes.

Monte Carlo simulations confirm the predicted trends of the mean field model: Strongly ionophilic pores show a monotonic decrease of capacitance with increasing pore size (Figure 2b), while weak ionophobicity produces a local maximum with capacitances comparable to, or even higher than, the capacitance at  $L \approx d$  (Figure 2c). The total ion packing fraction is almost constant with increasing pore width for strongly ionophilic pores (inset of Figure 2b) whereas for ionophobic pores it decreases with increasing pore width (inset of Figure 2c), agreeing qualitatively with the mean field model (inset of Figure 2a). We note that a slightly smaller  $\delta E$  in mean field theory is sufficient to achieve the same ion occupancy at zero voltage, hence ionophobicity, as in the Monte Carlo simulations. This discrepancy is due to the fact that our mean field theory does not account for the change in ion-image interactions due to ions positioning themselves off the central symmetry plane of the pore (though this effect does not change the qualitative predictions of the mean field model).

Another important aspect of capacitance optimization is how to choose the ion size ( $d$ ) and pore size ( $L$ ). Intuitively, one might expect that it is the *ratio* between the two that affects the capacitance. However, Figure 3a shows that for weakly ionophilic pores, a peak in the capacitance emerges as the ion diameter increases while the ratio between the pore size and the ion diameter,  $L/d$ , is kept fixed. This peak occurs because the ion self-energy and the metallic screening decrease (*i.e.* electrostatic interactions become stronger) when increasing

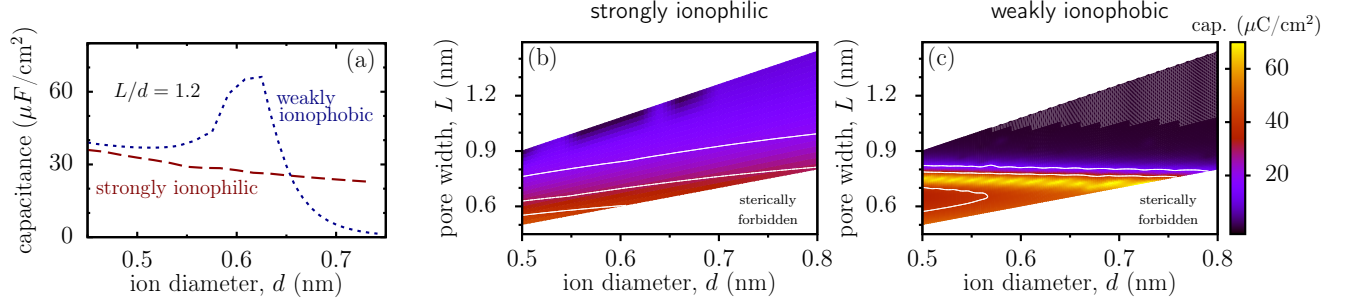


FIG. 3: (a) Capacitance at zero voltage as a function of ion diameter for weakly ionophobic ( $\delta E = 25k_B T$ ) and strongly ionophilic ( $\delta E = 10k_B T$ ) pores calculated using MFT. (b)-(c) Capacitance map for strongly and weakly ionophilic nanopores in the plane of ion diameter ( $d$ ) and the pore width ( $L$ ) calculated using MFT. This figure suggests a ‘two-step optimization strategy’, in which an optimal pair ( $d, L$ ) exists that maximizes the differential capacitance.

the ion diameter at constant  $L/d$  (see Eqs. (A3) and (A9) in Appendix A). This effect makes the pore less populated for weak ionophobilities, and thus adsorption of new counterions becomes entropically more favorable, giving rise to a local maximum at intermediate ion sizes. For strongly ionophilic pores, the ion density is close to maximal and charging proceeds mainly via swapping co-ions for counterions. Therefore, the capacitance increases monotonically with decreasing ion diameter (dashed line in Figure 3a).

From these results, we see that the largest possible capacitance may be obtained by optimizing *both* the pore width and the ion diameter (see Figure 3b and c). Crucially, the position of this optimum in parameter space, and its properties, depends on the pore’s ionophilicity.

The presence of a local maximum is distinct from the oscillatory behaviour of capacitance as a function of pore width [37, 40, 41] and solvent polarity [38] observed in systems with wider pores. For weakly ionophobic pores, a maximum occurs because of entropic effects, while in previous work, the pore is wider than a few ion diameters and it is the overlapping double layers that cause the non-monotonicity in the capacitance (notice a second maximum of similar origin in Figure 2(b), with small amplitude).

The fact that the capacitance reaches a maximum for relatively *wide* pores has an important impact on optimizing supercapacitors. It has previously been assumed that there must be a trade-off between having large capacitance (narrow pores) and fast charging (wide pores) [25]. Charging is slower for narrower pores because the collective (or effective) diffusion coefficient, which determines the rate of charging, decreases with decreasing pore width [25, 26, 42]. Our analysis therefore provides the key insight that charging kinetics and capacitance can be simultaneously optimized by tuning the ionophilicity of the pore.

#### IV. HYSTERETIC CHARGING

Next, we study the charging hysteresis for non-zero applied voltages. Figure 4 shows that charging can proceed via a first-order discontinuous phase transition at intermediate ionophilicities, or via a continuous process beyond the critical endpoints.

Figure 4a shows the capacitance as a function of applied voltage for ionophobic and ionophilic pores with no phase transition. For strongly ionophobic pores with resolution energy  $\delta E$  above the critical endpoint, the pore is initially empty and counter-ions will only enter the pore when the applied potential matches the unfavourable resolution energy; hence there is a peak in capacitance when charging starts at  $eV \approx \delta E$ . Subsequently, a separate regime of packing like charges starts and persists until the applied potential surpasses the interaction energy between co-ions. Beyond that point the capacitance falls off rapidly.

The situation is different for strongly ionophilic pores with  $\delta E$  below the critical endpoint. The pore is initially nearly fully occupied with ions. Charging occurs via *quid pro quo* swapping of co-ions for counter-ions due to the very strong resolution energy, and the charge density increases but the total density remains almost constant. Therefore, the capacitance is almost constant throughout charging, and only falls off when the co-ion density in the slit pore approaches zero. Indeed, recent NMR experiments [43, 44] show that charging proceeds continuously without phase transition and abrupt co-ion expulsion for KOH activated carbon pores, which are known to be strongly ionophilic [9]. While it is difficult to calculate the resolution energy (ionophobicity) for these pores, Figure 4c suggests that it must at least be lower than  $12k_B T$ . This is consistent with our estimate of the crossover between the ionophilic and ionophobic pores which occurs at  $\delta E_{\text{crossover}} \approx 17k_B T$  (see Section II).

For ionophilicities between the two critical endpoints, charging proceeds via a large discontinuous drop in density and capacitance (see Figure 4b). At low voltages, charging proceeds through swapping of co-ions for

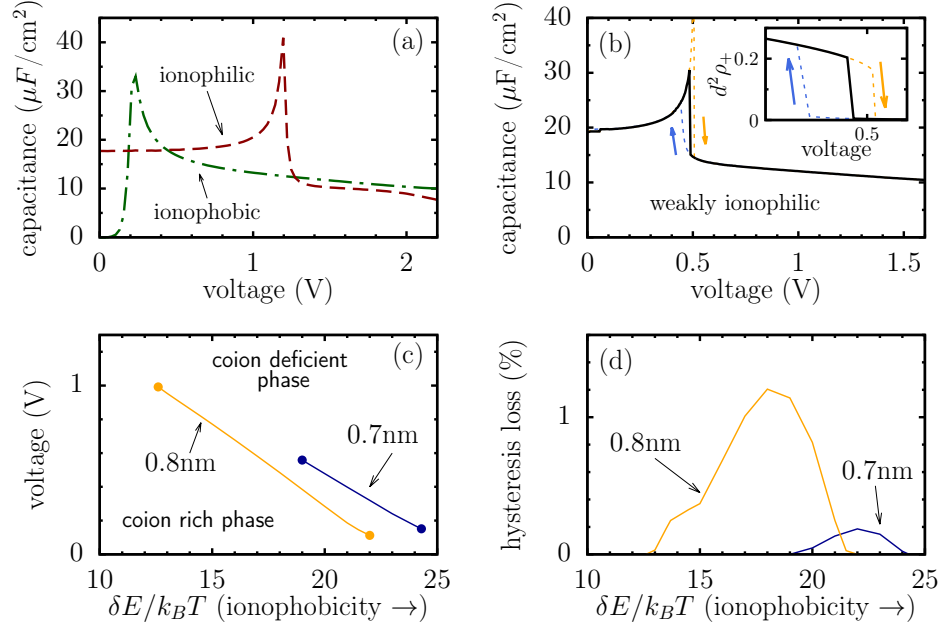


FIG. 4: Charging proceeds via a discontinuous phase transition for some parameter regimes. In all plots ion diameter  $d = 0.5\text{nm}$ , and the mean-field theory is used to compute the thermodynamic properties. (a) Capacitance as a function of voltage in the continuous charging regime. The ionophilic and -phobic pores have  $\delta E = 10k_B T$  and  $\delta E = 32k_B T$  respectively. (b) Capacitance as a function of voltage in the discontinuous charging regime. The solid curve indicates the minimum free energy path, and the dotted curves denote the hysteresis loop. The curve is plotted for  $\delta E = 18k_B T$ . The inset shows the abrupt expulsion of co-ions that drives the phase transition. (c) The phase diagram plotted for different slit widths. (d) The percentage of energy that is lost due to hysteresis during discharging of a nanopore charged at 1.3 volts (see Appendix A 4).

counter-ions and co-ion expulsion, but at the point of the phase transition the system discontinuously expels nearly all co-ions (see inset of Figure 4b), and beyond that point charging occurs via counter-ion adsorption. This voltage-induced abrupt expulsion of co-ions and the drop in total ion density has recently been observed in atomistic molecular dynamics simulations of [C2mim][FSI] and [C4mim][TFSI] ionic liquids in slit nanopores [33].

Figure 4c shows that the transition voltage increases with decreasing ionophobicity, as both counter ions and co-ions are favourably adsorbed into the pore, making it more difficult to expel the co-ions. The window of ionophilicities for which a phase transition occurs is wider for larger pores where electrostatic interactions are stronger and more long-ranged.

A signature of a discontinuous phase transition is hysteresis. The dotted lines in Figure 4b show that the branch followed by the system when the voltage is increased is different to that followed by the system for decreasing voltage. Figure 4d shows that a significant amount of energy is lost per cycle as a consequence of hysteresis, with wider pores producing larger energy losses. In practical applications, the regime where charging proceeds via a first order phase transition should therefore be avoided, but this hysteresis loop can be used to probe the properties of the supercapacitor system experimentally. It is likely however that these transitions will be smoothed out by the distribution of pore

sizes [45] in typically used porous electrodes (for instance in popular carbide-derived carbons [3]), making it difficult to capture them directly by *in situ* NMR spectroscopy [46, 47] or in electrochemical quartz crystal microbalance experiments [48, 49]. However, novel graphene and MXene-based nanoporous electrodes [6–8], which consist of nearly unimodal well-aligned slit pores with controllable pore widths, seem a promising candidate for validating our predictions experimentally.

## V. CONCLUSION

Using a mean-field model for charge storage in 2D nano-confinement and Monte Carlo simulations of the corresponding system in 3D, we have demonstrated the possibility of simultaneously boosting capacitance, accelerating charging, and avoiding hysteresis in nanoporous supercapacitors. Our analysis shows that the long-espoused paradigm that equates narrow pores with necessarily larger capacitance does not always hold: Entropic effects may produce a second, more pronounced peak in capacitance for relatively wide, ionophobic pores (Fig. 2). Similarly, there is an optimal ion diameter for weakly ionophilic pores, when the ratio between the ion diameter and pore width is kept constant (Fig. 3). For non-zero applied voltages, a voltage-induced discontinuous phase transition is predicted by the model, and the phase di-



agram has two critical endpoints corresponding to the limit of very ionophobic and ionophilic pores (Fig. 4). The phase transition gives rise to hysteresis and a sizeable energy loss, but crucially can be avoided by either reducing the operating voltage of the capacitor, or by pushing the pore ionophilicity away from the critical endpoints (for instance by making pores more ionophobic). Thus, the capacitance-power-hysteresis trilemma can be resolved by judicious tuning of material parameters and operating ranges.

Ion diameter and pore width are relatively straightforward to tune experimentally; our framework shows how to optimize both parameters together. Our model also singles out a key outstanding challenge for further experimentation — the controlled tuning of the ionophobicity/ionophilicity of the pore. The ionophilicity can be controlled by changing the ion-pore non-electrostatic interaction. In addition to van der Waals interactions, suppose we have an ion that has multiple conformational states with different effective diameters (for example expanded versus folded alkyl chains on an ionic liquid ion). If the pore separation is less than the effective diameter of the lowest energy conformation, then entering the pore will require the ion to adopt a higher conformational energy, and thus incur a conformational energy penalty. Similarly, if the pore walls are flexible and ions can only enter by deforming the walls (as observed in Refs. [50, 51]), the elastic energy will result in an unfavourable ion-pore non-electrostatic interaction. This interaction could also be controlled by addition of surfactants [52, 53] to ionic liquids or by using ionic liquid mixtures [54], or via functionalisation of porous carbons [9]. Experimental studies of ionophilicity are currently scarce, however, and we hope that our theory will provide a framework to assess and direct future efforts to address this.

### Acknowledgments

This work is supported by an EPSRC Doctoral Training Award to AAL. SK acknowledges COST Action MP1004 for supporting his short-time scientific visit to Imperial College London where part of this work has been done. Fruitful discussions with Alexei Kornyshev (Imperial College) are appreciated.

### Appendix A: Improved mean-field approximation

The Helmholtz free energy  $F(\rho_+, \rho_-)$  per unit area of a homogeneous ionic liquid in a narrow slit nanopore is given by

$$\beta F = U_{\text{el}}(\rho_+, \rho_-) - S(\rho_+, \rho_-) + \sum_{\alpha=\pm} h_{\alpha} \rho_{\alpha}, \quad (\text{A1})$$

where  $\beta = (k_B T)^{-1}$  ( $k_B$  is the Boltzmann constant and  $T$  temperature),  $\rho_{\pm}$  are the two-dimensional ion densities,

and it is convenient to introduce  $\rho = \rho_+ + \rho_-$  and  $c = \rho_+ - \rho_-$ .  $k_B T U_{\text{el}}$  is the contribution to free energy due to electrostatic interactions,  $k_B T S$  is the excluded volume entropic contribution, and  $k_B T h_{\alpha}$  is the electrochemical potential of the ion species (see below).

### 1. Electrostatic interactions

The electrostatic interaction can be expressed in terms of direct correlation functions  $\mathcal{C}_{\alpha\beta}(x, x')$  using a functional Taylor expansion

$$U_{\text{el}}(\rho_+, \rho_-) \approx \sum_{\alpha, \beta=\pm} \int dx \int dx' \mathcal{C}_{\alpha\beta}(x, x') \rho_{\alpha} \rho_{\beta}, \quad (\text{A2})$$

with  $\mathcal{C}_{\alpha\beta}(x, x')$  computed using the Ornstein-Zernicke relation with an appropriate closure [55]. However, we take here a simplifying assumption in the spirit of the random phase approximation (RPA). In RPA, the direct correlation function is approximated by the interaction potential, which is valid for asymptotically weak interactions but overestimates the correlations at close particle separations [55]. To improve on this, we assume that the direct correlation function is essentially negligible for distances less than the average particle separation; beyond this distance the interaction is weak and can be approximated by the classical RPA. As such,  $\mathcal{C}_{\alpha\beta}(x, x') \approx v_{\alpha\beta}(x - x') \theta(|x - x'| - R_c)$  where  $v_{\alpha\beta}(x - x')$  is the electrostatic interaction kernel and  $R_c = 1/\sqrt{\pi\rho}$  is the average separation between particles (this result is also known as the cut-out disc approximation, see Ref. [56]).

The interaction potential between two point charges confined in a slit metallic nanopore and separated by distance  $r$  is given by [57]

$$v_{\alpha\beta}(r, z_1, z_2) = \frac{4q_{\alpha}q_{\beta}}{\varepsilon_p L} \sum_{n=1}^{\infty} K_0(\pi n r/L) \sin(\pi n z_1/L) \sin(\pi n z_2/L), \quad (\text{A3})$$

where  $q_{\alpha}$  and  $q_{\beta}$  are charges,  $\varepsilon_p$  the dielectric constant in the pore, and  $z_1$  and  $z_2$  are ion positions across the pore (within the mean-field model we assume  $z_{1,2} = L/2$ , but we use the full potential in our Monte Carlo simulations, see below). For monovalent ions, we therefore have [15]

$$U_{\text{el}}(c, \rho) = 4c^2 R_c(\rho) l_B \sum_{n=1}^{\infty} \frac{\sin^2(\pi n/2)}{n} K_1(\pi n R_c(\rho)/L), \quad (\text{A4})$$

where  $l_B = e^2/(\varepsilon_p k_B T)$  is the thermal Bjerrum length. Constrained ionic motion within the pore means that effectively only electronic degrees of freedom contribute to dielectric screening and we take  $\varepsilon_p = 2$ , the high frequency dielectric constant of typical ionic liquids. It is easy to see that at constant  $L/d$ , the functional dependence of the potential  $v_{\alpha\beta}$  on  $d$  is the same as on  $L$  at constant  $d$ .

## 2. Entropic contributions

The entropic contribution in Eq. (A1) is modelled here based on the analytically solvable 2D scaled particle theory. The typical pore separation is only slightly larger than the ion diameter, and thus we can take into account the positional disorder of ions normal to the pore surface as a perturbation to the otherwise 2D system — this effectively renormalizes the ion diameter. Thus the entropy is given as a sum of the ideal gas contribution and hard core exclusion,

$$S(\rho_+, \rho_-) = \sum_{\alpha=\pm} \tilde{\rho}_\alpha \ln \tilde{\rho}_\alpha + \tilde{\rho} \left[ \frac{\tilde{\eta}^2}{1 - \tilde{\eta}} - \ln(1 - \tilde{\eta}) \right], \quad (\text{A5})$$

where  $\tilde{\eta}(\rho) = \pi\rho\sigma^2/4 = \pi\tilde{\rho}d^2/4$  is the effective ion packing fraction and  $\sigma(d, L, \rho)$  is a renormalized diameter that accounts for the out-of-plane packing of ions. Schmidt and Löwen [58, 59] showed that

$$\sigma^2(d, L, \rho) = d^2 + \frac{1}{\alpha(\rho)} - \frac{L \exp(\alpha(\rho)L^2/4)}{\sqrt{\pi\alpha(\rho)} \operatorname{erfi}(\sqrt{\alpha(\rho)}L/2)} \quad (\text{A6})$$

where  $\operatorname{erfi}(z)$  is the imaginary error function, and

$$\alpha(\rho) = \pi\rho g(\rho) = \pi\rho \frac{1 - \tilde{\eta}(\rho)/2}{(1 - \tilde{\eta}(\rho))^2} \quad (\text{A7})$$

is the average density at contact and  $g(\rho)$  the 2D pair correlation function evaluated at contact.

## 3. Electrochemical potential

The electrochemical potential is given by

$$h_\pm = \pm u + \delta E_{\text{self}} + \delta E_\pm = \pm u - \frac{l_B}{L} \ln 2 + \delta E_\pm. \quad (\text{A8})$$

Here the first term results from the applied voltage, and the second term originates from the ion self energy

$$\begin{aligned} \delta E_{\text{self}}(z) &= \lim_{r \rightarrow 0} \left( \phi(r) - \frac{1}{r} \right) \\ &= \frac{l_B}{L} \int_0^\infty \left[ \frac{\sinh(Q(1 - z/L)) \sinh(Qz/L)}{\sinh(Q)} \right. \\ &\quad \left. - \frac{1}{2} \right] dQ, \end{aligned} \quad (\text{A9})$$

where  $z$  is the position across the pore and  $r$  distance to the charge (see Ref. [15]). At the pore mid plane  $z = L/2$  which gives  $\delta E_{\text{self}}(L/2) = -l_B \ln(2)/L$ . Again,  $\delta E_{\text{self}}$  depends on  $L$  in the same way as on  $d$  at constant  $L/d$ . The last term in Equation (A8),  $\delta E_\pm$ , is the “resolution energy” which includes the bulk chemical potential.

## 4. Hysteretic energy loss

The energy (per surface area) stored in a nanopore by charging it from  $u = u_1$  to  $u = u_2$  is

$$\mathcal{E}(u_1, u_2) = \int_{u_1}^{u_2} u C_D(u) du, \quad (\text{A10})$$

where  $C_D(u) = dQ/dV$  is differential surface-specific capacitance. To obtain an energy lost due to hysteresis (Figure 4d), we first calculated the energy stored when charging a nanopore from  $u_1 = 0$  to  $u_2 = V = 1.3$  V along the charging path (orange lines/arrows in Figure 4b),  $\mathcal{E}_{\text{charg}} = \mathcal{E}(0, V)$ ; and the energy released by fully discharging it along the discharging path (blue lines/arrows in Figure 4b),  $\mathcal{E}_{\text{discharg}} = -\mathcal{E}(V, 0)$ . The hysteric energy loss is then shown as percentage of the stored energy lost in hysteresis, i.e.  $(\mathcal{E}_{\text{charg}} - \mathcal{E}_{\text{discharg}})/\mathcal{E}_{\text{charg}}$ .

## Appendix B: Grand canonical Monte Carlo simulations

We used the same method as in Ref. [34], so we will only summarize the simulation method here, and refer the reader to [34] for further detail.

Ionic liquid molecules are modelled as charged hard spheres, but instead of the Coulomb potential, we use the analytical solution (A3) for the ion-ion interactions. Ion-pore wall interactions are captured by potential (A9), accounting for image forces. The resolution energy ( $\delta E$ ) and the applied voltage ( $V$ ) are subsumed into the chemical potential in the grand canonical simulations,  $\mu_\pm^{(\text{sim})} = \delta E \pm eV$ , where  $e$  is the elementary charge, and  $\delta E$  contains the chemical potential of ions in the bulk of a supercapacitor. In all our simulations we took temperature  $T = 328$  K and the relative dielectric constant inside pores  $\varepsilon_p = 2$ .

To calculate differential capacitance, we differentiated the accumulated charge obtained from Monte Carlo simulations with respect to voltage numerically using the Holoborodko method with seven points [60, 61].

- 
- [1] M. Lu, F. Beguin, and E. Frackowiak, *Supercapacitors: Materials, Systems and Applications* (John Wiley & Sons, 2013).
  - [2] P. Simon and Y. Gogotsi, *Acc. Chem. Res.* **46**, 1094 (2013).
  - [3] P. Simon and Y. Gogotsi, *Nature Mater.* **7**, 845 (2008).

- [4] E. Frackowiak, *Phys. Chem. Chem. Phys.* **9**, 1774 (2007).
- [5] Y. Gogotsi, A. Nikitin, H. Ye, W. Zhou, J. E. Fischer, B. Yi, H. C. Foley, and M. W. Barsoum, *Nat. Mater.* **2**, 591 (2003).
- [6] J. J. Yoo, K. Balakrishnan, J. S. Huang, V. Meunier, B. G. Sumpter, A. Srivastava, M. Conway, A. L. M.

- Reddy, J. Yu, R. Vajtai, et al., *Nano Lett.* **11**, 1423 (2011).
- [7] X. Yang, C. Cheng, Y. Wang, L. Qiu, and D. Li, *Science* **341**, 534 (2013).
- [8] M. R. Lukatskaya, O. Mashtalir, C. E. Ren, Y. Dal-Agnese, P. Rozier, P. L. Taberna, M. Naguib, P. Simon, M. W. Barsoum, and Y. Gogotsi, *Science* **341**, 1502 (2013).
- [9] F. W. Richey, C. Tran, V. Kalra, , and Y. A. Elabd, *J. Phys. Chem. C* **118**, 21846 (2014).
- [10] B. Conway, *Electrochemical supercapacitors: scientific fundamentals and technological applications* (Springer, 1999).
- [11] E. Raymundo-Piñero, K. Kierczek, J. Machnikowski, and F. Béguin, *Carbon* **44**, 2498 (2006).
- [12] J. Chmiola, G. Yushin, Y. Gogotsi, C. Portet, P. Simon, and P. Taberna, *Science* **313**, 1760 (2006).
- [13] C. Largeot, C. Portet, J. Chmiola, P. Taberna, Y. Gogotsi, and P. Simon, *J. Am. Chem. Soc.* **130**, 2730 (2008).
- [14] R. Lin, P. Huang, J. Segalini, C. Largeot, P.-L. Taberna, J. Chmiola, Y. Gogotsi, and P. Simon, *Electrochim. Acta* **54**, 7025 (2009).
- [15] S. Kondrat and A. Kornyshev, *J. Phys.: Condens. Matter* **23**, 022201 (2011).
- [16] C. C. Rochester, A. A. Lee, G. Pruessner, and A. A. Kornyshev, *ChemPhysChem* **16**, 4121 (2013).
- [17] A. Goduljan, F. Juarez, L. Mohammadzadeh, P. Quaino, E. Santos, and W. Schmickler, *Electrochem. Comm.* (2014).
- [18] L. Mohammadzadeh, A. Goduljan, F. Juarez, P. Quaino, E. Santos, and W. Schmickler, *Electrochim. Acta* (2015).
- [19] C. Merlet, B. Rotenberg, P. A. Madden, P.-L. Taberna, P. Simon, Y. Gogotsi, and M. Salanne, *Nature Mater.* **11**, 306 (2012).
- [20] C. Merlet, C. Péan, B. Rotenberg, P. A. Madden, B. Daffos, P.-L. Taberna, P. Simon, and M. Salanne, *Nature Comm.* **4**, 2701 (2013).
- [21] P. Wu, J. Huang, V. Meunier, B. Sumpster, and R. Qiao, *ACS Nano* **5**, 9044 (2011).
- [22] R. Qiao, V. Meunier, and B. Sumpster, *J. Phys. Chem. Lett.* **3**, 1732 (2012).
- [23] J. Vatamanu, Z. Hu, D. Bedrov, C. Perez, and Y. Gogotsi, *J. Phys. Chem. Lett.* **4**, 2829 (2013).
- [24] R. Mysyk, E. Raymundo-Piñero, and F. Béguin, *Electrochem. Comm.* **11**, 554 (2009).
- [25] S. Kondrat and A. Kornyshev, *J. Phys. Chem. C* **117**, 12399 (2013).
- [26] S. Kondrat, P. Wu, R. Qiao, and A. A. Kornyshev, *Nature Mater.* **13**, 387 (2014).
- [27] V. Lockett, R. Sedev, J. Ralston, M. Horne, and T. Rodopoulos, *J. Phys. Chem. C* **112**, 7486 (2008).
- [28] W. Zhou, S. Inoue, T. Iwahashi, K. Kanai, K. Seki, T. Miyamae, D. Kim, Y. Katayama, and Y. Ouchi, *Electrochem. Comm.* **12**, 672 (2010).
- [29] A. Uysal, H. Zhou, G. Feng, S. S. Lee, S. Li, P. Fenter, P. T. Cummings, P. F. Fulvio, S. Dai, J. K. McDonough, et al., *J. Phys. Chem. C* **118**, 569 (2013).
- [30] M. Drüschler, B. Huber, S. Passerini, and B. Roling, *J. Phys. Chem. C* **114**, 3614 (2010).
- [31] K. Kiyohara, T. Sugino, and K. Asaka, *J. Chem. Phys.* **134**, 154710 (2011).
- [32] L. Xing, J. Vatamanu, O. Borodin, and D. Bedrov, *J. Phys. Chem. Lett.* **4**, 132 (2013).
- [33] J. Vatamanu, M. Vatamanu, and D. Bedrov, *ACS nano* p. Article ASAP (2015).
- [34] S. Kondrat, N. Georgi, M. Fedorov, and A. Kornyshev, *Phys. Chem. Chem. Phys.* **13**, 11359 (2011).
- [35] K. Kiyohara, H. Shioyama, T. Sugino, and K. Asaka, *J. Chem. Phys.* **136**, 094701 (2012).
- [36] K. Kiyohara, H. Shioyama, T. Sugino, K. Asaka, Y. Soneda, K. Imoto, and M. Kodama, *J. Chem. Phys.* **138**, 234704 (2013).
- [37] D. Jiang, Z. Jin, and J. Wu, *Nano Lett.* **11**, 5373 (2011).
- [38] D. Jiang and J. Wu, *Nanoscale* **6**, 5545 (2014).
- [39] J. F. Jover, R. Lugo, H. Toulhoat, P. Simon, and T. De Bruin, *J. Phys. Chem. C* **118**, 864 (2014).
- [40] G. Feng and P. Cummings, *J. Phys. Chem. Lett.* **2**, 2859 (2011).
- [41] O. Pizio, S. Sokolowski, and Z. Sokolowska, *J. Chem. Phys.* **137**, 234705 (2012).
- [42] A. A. Lee, S. Kondrat, G. Oshanin, and A. A. Kornyshev, *Nanotechnology* **25**, 315401 (2014).
- [43] J. M. Griffin, A. C. Forse, H. Wang, N. M. Trease, P.-L. Taberna, P. Simon, and C. P. Grey, *Faraday Discuss.* (2014), accepted.
- [44] J. M. Griffin, A. C. Forse, W.-Y. Tsai, P.-L. Taberna, P. Simon, and C. P. Grey (2015), submitted.
- [45] S. Kondrat, C. R. Pérez, V. Presser, Y. Gogotsi, and A. A. Kornyshev, *Energy Environ. Sci.* **5**, 6474 (2012).
- [46] H. Wang, A. C. Forse, J. M. Griffin, N. M. Trease, L. Trognko, P.-L. Taberna, P. Simon, and C. P. Grey, *J. Am. Chem. Soc.* **135**, 18968 (2013).
- [47] A. C. Forse, J. M. Griffin, H. Wang, N. M. Trease, V. Presser, Y. Gogotsi, P. Simone, and C. P. Grey, *Phys Chem Chem Phys* **15**, 7722 (2013).
- [48] M. D. Levi, G. S. N. Levy, D. Aurbach, and J. Maier, *Nat. Mater.* **8**, 872 (2009).
- [49] W.-Y. Tsai, P.-L. Taberna, and P. Simon, *J. Am. Chem. Soc.* **136**, 8722 (2014).
- [50] F. Kaasik, T. Tamm, M. Hantel, E. Perre, A. Aabloo, E. Lust, M. Bazant, and V. Presser, *Electrochem. Comm.* **34**, 196 (2013).
- [51] M. Hantel, D. Weingarth, and R. Kötz, *Carbon* **69**, 275 (2014).
- [52] K. Fic, G. Lot, and E. Frackowiak, *Electrochim. Acta* **55**, 7484 (2010).
- [53] K. Fic, G. Lot, and E. Frackowiak, *Electrochim. Acta* **60**, 206 (2011).
- [54] R. Lin, P.-L. Taberna, S. Fantini, V. Presser, C. R. Pérez, F. Malbosc, N. L. Rupesinghe, K. B. K. Teo, Y. Gogotsi, and P. Simon, *J. Phys. Chem. Lett.* **2**, 2396 (2011).
- [55] J.-P. Hansen and J. R. MacDonald, *Theory of Simple Liquids* (Elsevier, 2014), 4th ed.
- [56] A. A. Kornyshev and W. Schmickler, *J. Electroanal. Chem.* **202**, 1 (1986).
- [57] W. R. Smythe, *Static and Dynamic Electricity* (McGraw Hill, 1939).
- [58] M. Schmidt and H. Löwen, *Phys. Rev. Lett.* **76**, 4552 (1996).
- [59] M. Schmidt and H. Löwen, *Phys. Rev. E* **55**, 7228 (1997).
- [60] S. Kondrat, A. Kornyshev, F. Stoeckli, and T. A. Centeno, *Electrochem. Comm.* **34**, 348 (2013).
- [61] P. Holoborodko, *Smooth noise robust differentiators*, <http://www.holoborodko.com/pavel/numerical-methods/numerical-derivative/smooth-low-noise-differentiators/> (2008).
- [62] M. Bier and S. Dietrich, *Mol. Phys.* **108**, 211 (2010).



- [63] Ref. [39] accounts for enthalpic contributions only; the entropic contribution can be estimated via the Trouton rule, where the entropy of vapourization  $\Delta_v S \approx (95 \pm 10) \text{J mol}^{-1}$  (see Ref. [62]).
- [64] Estimate obtained from Ref. [39], where a cylindrical geometry is studied. Our estimate is obtained by taking the large radius asymptotic value of the ion-

wall van der Waals interaction energy, *i.e.*  $E_{\text{vdw,slit}} \approx 2E_{\text{vdw,cylinder}}(R \rightarrow \infty)$ , as the  $R \rightarrow \infty$  asymptotic value of the van der Waals interaction energy corresponds to the interaction energy between an ion and one side of the pore.